

A Three-dimensional Adaptive Strategy with Uniform Background Grid in Element-free Galerkin Method for Extremely Large Deformation Problems

Cheng-Te Chi¹, Ming-Hsiao Lee² and Wen-Hwa Chen^{1,3}

Abstract: A novel three-dimensional adaptive element-free Galerkin method (EFGM) based on a uniform background grid is proposed to cope with the problems with extremely large deformation. On the basis of this uniform background grid, an interior adaptive strategy through an error estimation within the analysis domain is developed. By this interior adaptive scheme, additional adaptive nodes are inserted in those regions where the solution accuracy needs to be improved. As opposed to the fixed uniform background grid, these inserted nodes can move along with deformation to describe the particular local deformation of the structure. In addition, a triangular surface technique is adopted to depict the geometry of the three-dimensional structure and a new surface adaptive strategy on the surface of the structure is also proposed. The complicated geometry of the three-dimensional structure can be thus analyzed precisely even under extremely large deformation. Besides, the contact regions of the structure can be determined accurately when the contact behavior occurs. Therefore, the present EFGM adaptive strategy not only retains the advantage of the uniform background grid for solving the extremely deformed problems, but also enhances the solution accuracy in the interior and surface of the structure.

Two three-dimensional problems, say, the upsetting of a cylinder and the embossing process of microimprint lithography, are undertaken to demonstrate the versatility and efficiency of this novel adaptive EFGM analysis procedure with the uniform background grid. It is noteworthy that the present adaptive strategies can also be generally applied to other meshless methods, such as the meshless local Petrov-Galerkin method, etc.

¹ Dept. of Power Mech. Engng., National Tsing Hua University, Hsinchu, Taiwan, Republic of China

² National Center for High-performance Computing, National Applied Research Laboratories, Hsinchu, Taiwan, Republic of China

³ National Applied Research Laboratories, Taipei, Taiwan, Republic of China

Keywords: Element-Free Galerkin Method, Adaptive Analysis, Large Deformation, Background Grid

1 Introduction

The meshless methods, such as the element-free Galerkin method (Belytschko et al. 1994; Chen and Guo, 2001; Chen and Chen, 2005; Chen et al., 2009; Lee and Chen, 2009) and the meshless local Petrov-Galerkin method (MLPG) (Atluri and Zhu, 1998; Atluri, 2004; Li and Atluri, 2008), have achieved outstanding success in dealing with various scientific and engineering problems in the decade. Since the interpolation functions of the sub-domain in the meshless methods are derived merely by a set of scattering nodes without any element connectivity, nodes can be simply inserted, rearranged or discarded, especially for three-dimensional problems. This merit makes the meshless methods particularly adequate for the adaptive analysis.

Nagashima (2000) built the adaptive analysis by a node-by-node meshless method. By this adaptive scheme, the solution accuracy of the central node within the sub-domain is improved by an error estimation and additional nodes are inserted at the center points between the central node and its neighboring influencing nodes, as shown in Fig.1 (a). Similar concept was adopted by Zhang et al. (2005). Nevertheless, Rabczuk and Belytschko (2005) utilized the integration cells based error estimation. With this error estimation, if the error of an integration cell is beyond the predetermined tolerance, this integration cell will be divided into four sub-cells and the new nodes are introduced at the vertexes of these sub-cells, as illustrated in Fig.1 (b). Chung (2000), Jun and Im (2000) and Rossi and Alves (2005) also refined the integration cells in somewhat similar ways to achieve the purpose of adaptivity. Liu and Tu (2002) proposed their adaptive meshless method for two-dimensional problems by introducing new nodes through the Delaunay triangular technique. By this technique, the analysis domain to be solved is adaptively meshed by the Delaunay triangles based on the existing nodes which are located on the vertexes of these Delaunay triangles. As drawn in Fig.1 (c), once the new nodes for adaptivity are inserted, more Delaunay triangles with existing and inserted nodes at the vertexes are induced. Another adaptive meshless method which employs the Voronoi plot scheme was proposed by Lu and Chen (2002). By this scheme, each node has its corresponding Voronoi polygon cell. For the analysis domain discretized by n distinct nodes, as depicted in Fig.1 (d), n Voronoi polygon cells are constructed. The sides of the Voronoi polygon cell for a certain node perpendicularly bisect the lines connecting this node and its adjacent neighboring nodes. Therefore, a Voronoi polygon cell is uniquely defined to each node. If the error estimation for a node is unsatisfied, additional nodes for adaptivity are inserted at all the vertexes

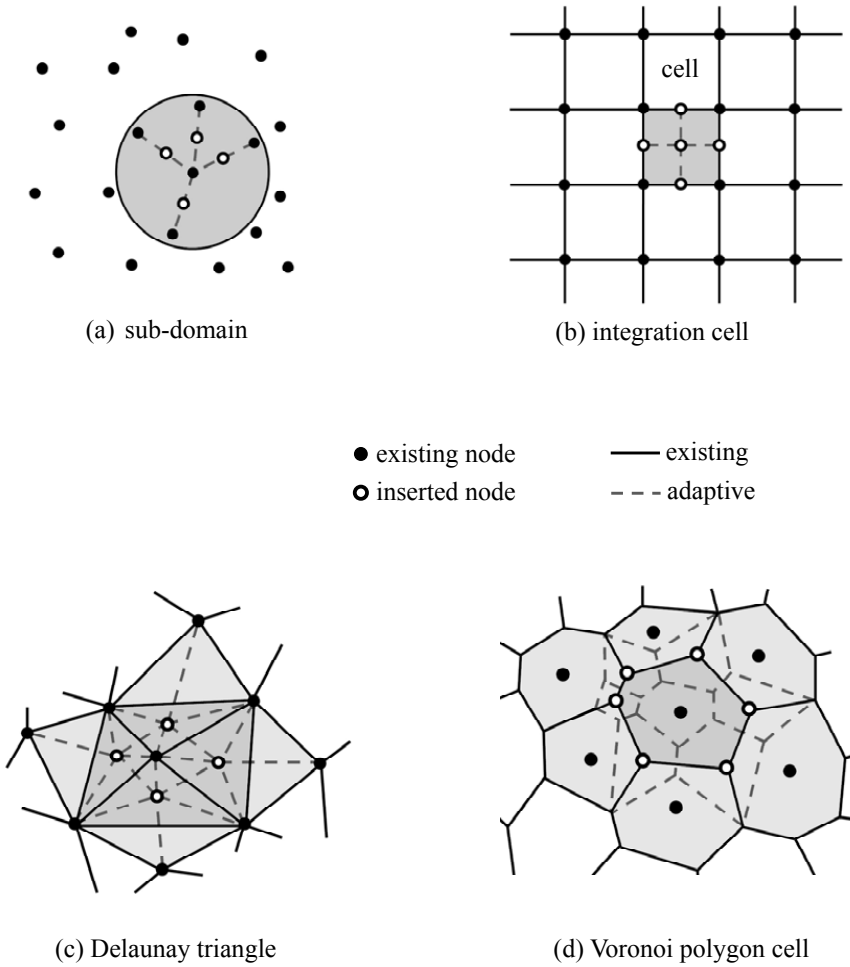


Figure 1: Several developed adaptive schemes

of its corresponding Voronoi polygon cell. Notice that after the reconstruction of the Voronoi polygon cells is accomplished, each node, no matter existing node or inserted node, still possesses its corresponding Voronoi polygon cell. Moreover, You et al. (2003), Liu et al. (2006), Yvonnet et al. (2006), Li and Lee (2006) and Rabczuk and Belytschko (2007) also utilized the concept of the Voronoi plot to construct their adaptive meshless methods to solve a variety of problems. Although these above-mentioned adaptive meshless methods show their advantages in many engineering fields, only increasing the nodal density in some particular regions is still inadequate to deal with the extremely distorted nodal distribution resulting

from the truly large deformation. Further, in the latter two adaptive meshless methods, the reestablishment of the Delaunay triangles or Voronoi polygon cells is necessary once the new nodes are inserted within the analysis domain. Consequently, the computational work inherently increases.

The uniform background grid has been proven its versatility in coping with the severely distorted nodal distribution (Chen et al., 2009). Nevertheless, the solution accuracy in some regions by the whole uniform background grid may be sometimes unsatisfied. Although it will probably be improved by refining the whole uniform background grid, the considerably additional degrees of freedom will significantly increase the computational cost. However, the uniform background grid in conjunction with an adaptive strategy may be an effective approach to achieve solution accuracy and efficiency simultaneously. The purpose of this work is thus to develop a new adaptive EFGM analysis procedure through the uniform background grid to tackle the three-dimensional problems with extremely large deformation. The adaptive strategy includes the interior and surface adaptivity of the analysis domain. For the proposed interior adaptivity, new nodes can be inserted in some regions to boost the solution accuracy within the analysis domain by an error estimation. As opposed to the interior nodes in the uniform background grid, the inserted nodes within the analysis domain can move with the deformation to capture specific structural behaviors accurately. In addition, to describe the geometry of three-dimensional structure, a surface adaptive strategy based on a triangular surface scheme (Lee and Chen, 2010) is also proposed through refining the triangular surfaces representing the surface of the structure. Hence, this proposed adaptive EFGM analysis procedure not only retains the merit of the uniform background grid in overcoming the difficulty resulting from the truly large deformation, but also improves the solution accuracy in some regions which are calculated only by the whole uniform background grid.

Finally, to display the efficiency and versatility of the adaptive EFGM analysis procedure developed, the three-dimensional examples, including the upsetting of a cylinder and the embossing process of microimprint lithography, are analyzed. The present computed results well agree with those available in the literatures.

2 Incremental Formulation of Element-Free Galerkin Method

In order to accurately account for the geometrical and material nonlinear effects due to extremely large deformation during loading process, an incremental approach of element-free Galerkin method with uniform background grid has been successfully established by the authors (Chen et al., 2009) and is also adopted in this work. Consider a three-dimensional structure $\Omega^{(N)}$ enclosed by the boundary $\Gamma^{(N)}$ at $C^{(N)}$ state as shown in Fig.2. Based on the principle of minimum total potential energy, as well

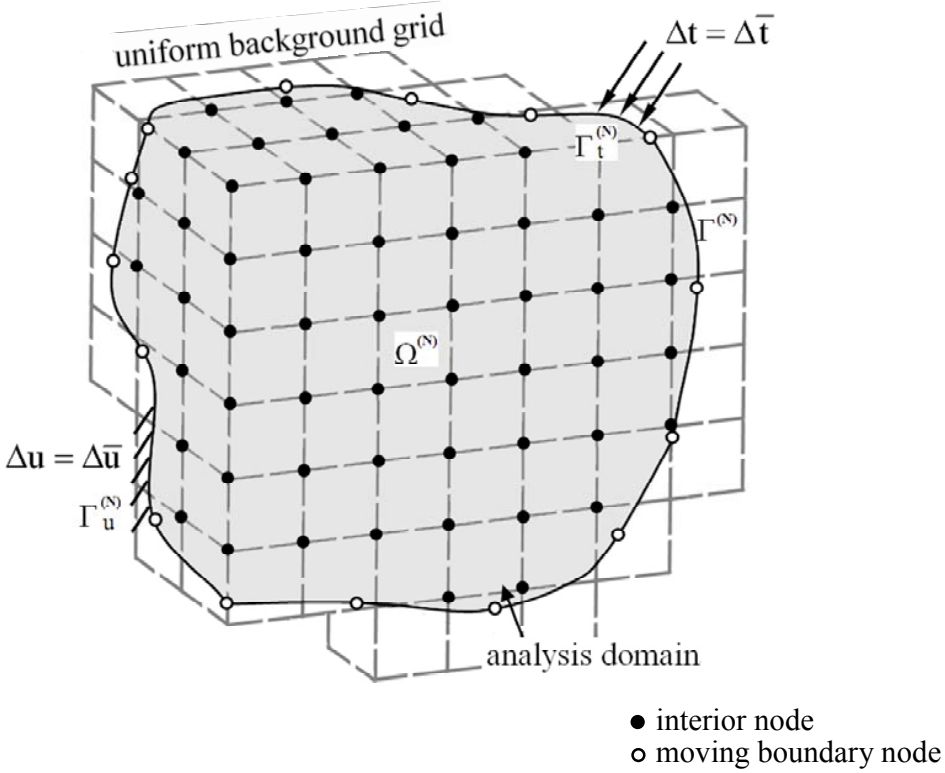


Figure 2: An incremental three-dimensional EFGM analysis model (Chen et al., 2009)

derived in the earlier work (Chen et al., 2009), the incremental functional $\Delta\Pi$ from $C^{(N)}$ state to $C^{(N+1)}$ state is quoted as follows (neglecting the body force effect):

$$\begin{aligned} \Delta\Pi(\Delta u_i) &= \int_{\Omega^{(N)}} \left(\frac{1}{2} E_{ijkl} \Delta e_{ij} \Delta e_{kl} + \frac{1}{2} \tau_{ij}^{(N)} \Delta u_{k,i} \Delta u_{k,j} \right) d\Omega - \int_{\Gamma_t^{(N)}} \Delta \bar{t}_i \Delta u_i d\Gamma \\ &\quad - \left[\int_{\Gamma_u^{(N)}} \bar{t}_i^{(N)} \Delta u_i d\Gamma - \int_{\Omega^{(N)}} \tau_{ij}^{(N)} \Delta e_{ij} d\Omega \right] \\ &= \min. \end{aligned} \tag{1}$$

It is assumed that all the state quantities, such as the nodal displacements, stresses and strains from $C^{(0)}$ state to $C^{(N)}$ state, are already gained. Δu_i and Δe_{ij} represent the incremental displacements and linearized incremental Green-Lagrangian strains from $C^{(N)}$ state to $C^{(N+1)}$ state, respectively. E_{ijkl} is the current constitu-

tive property tensor. Besides, $\bar{t}_i^{(N)}$ and $\Delta\bar{t}_i$ are defined as the prescribed surface tractions acting on the traction boundary $\Gamma_t^{(N)}$ at $C^{(N)}$ state and its corresponding increments from $C^{(N)}$ state to $C^{(N+1)}$ state, respectively. $\tau_{ij}^{(N)}$ presents the Cauchy (true) stresses at $C^{(N)}$ state. Since the piecewise linear incremental process is taken to approximate the nonlinear behaviors, the last two terms indicated in the bracket [] in Eqn. (1) are retained to serve as an equilibrium check.

Subsequently, the incremental displacements and linearized incremental Green-Lagrangian strains from $C^{(N)}$ state to $C^{(N+1)}$ state can be discretized as incremental nodal displacements through a moving least square (MLS) approximation (Belytschko et al., 1994). The incremental governing equations of the analysis domain from $C^{(N)}$ state to $C^{(N+1)}$ in matrix form are obtained by applying the stationary condition of $\Delta\Pi$ with respect to the incremental nodal displacements of all the nodes $\{\Delta q^*\}$ within the analysis domain from $C^{(N)}$ state to $C^{(N+1)}$ state, say,

$$([K_M] + [K_G])\{\Delta q^*\} = \{\Delta Q\} + \{\Delta Q^*\}. \quad (2)$$

As expressed in Eqn. (2), $[K_M]$ and $[K_G]$ denote the incremental stiffness matrix of the analysis domain at $C^{(N)}$ state, which represent the material nonlinearity and geometric nonlinearity due to severely large deformation, respectively. $\{\Delta Q\}$ refers to the incremental external load vector from $C^{(N)}$ state to $C^{(N+1)}$ state and $\{\Delta Q^*\}$ is the equilibrium check vector calculated at $C^{(N)}$ state. Without loss of generality, the integration cells (Belytschko et al., 1994), employed in the conventional EFGM for performing the numerical integration of respective matrix as expressed in Eqn. (2), can also be arranged to coincide with part of the uniform background grid for simplicity.

3 Adaptivity with Uniform Background Grid

As mentioned earlier, although the incremental EFGM analysis procedure with uniform background grid can deal with the three-dimensional problems with extremely large deformation (Chen et al., 2009), an efficient adaptive scheme is still required to improve the solution accuracy in particular regions. The novel adaptive strategy proposed here comprises the interior and surface adaptivity of the analysis domain with arbitrary geometric shape. The interior adaptivity is developed with the uniform background grid (Chen et al., 2009) for the interior of the analysis domain and the surface adaptivity is grounded on the triangular surface scheme (Lee and Chen, 2010) for the surface of the analysis domain, both will be introduced thereafter.

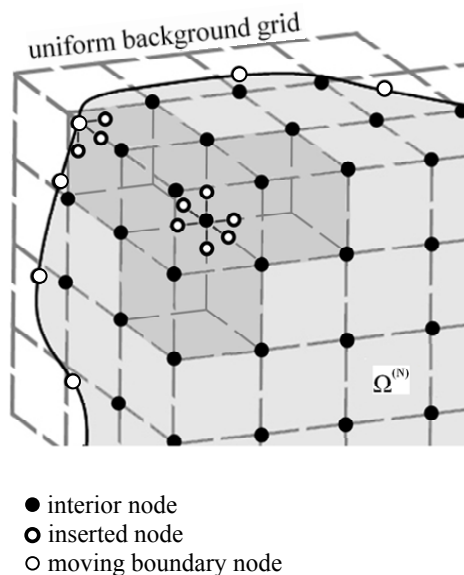


Figure 3: The interior adaptive scheme with uniform background grid

3.1 Interior Adaptive Strategy

As shown in Fig. 2, Chen et al. (2009) discretized the three-dimensional deformable analysis domain $\Omega^{(N)}$ enclosed by its boundary $\Gamma^{(N)}$ by two kinds of nodes, say, the moving boundary nodes staying with the boundary and the interior nodes selected from part of the uniform background grid. When an incremental loading is applied while the relative error for an interior node estimated by the error estimation exceeds a predetermined tolerance, the interior adaptivity needs to be done and the third kind of nodes is introduced. As displayed in Fig. 3, 6 additional adaptive nodes for an interior node are inserted on both sides of three mutually perpendicular edges of the uniform background grid, respectively. The distances between this interior node and the inserted nodes on the edges are taken as quarters of the spacing of the uniform background grid. However, if the adaptivity is performed around a moving boundary node, only the adaptive nodes within the deformable analysis domain are added. Therefore, the number of the inserted nodes for a moving boundary node can be from 1 to 5.

Unlike the fixed fictitious nodes comprising the uniform background grid, all the moving boundary nodes and the inserted nodes will move in the uniform background grid to describe the deformation behavior during the loading process for adaptivity. Notice that if an inserted node for adaptivity is very close to the inte-

rior or moving boundary node due to deformation during the loading process, it had better be discarded to avoid possible computational illness. Similarly, if a new inserted node is close to the adaptive node inserted within the analysis domain in the previous states, this new inserted node will be eliminated to avert over-crowded nodal distribution.

To achieve the interior adaptivity, an error estimation is essentially necessary. The simple and robust error estimation proposed by Chung and Belytschko (1998) is thus adopted. Because the derivatives of the interpolation functions may introduce spurious oscillations in EFGM stress field in some regions (Chung and Belytschko, 1998), another smoother stress field is calculated through the stress projection technique. Based on the MLS approximation (Chen et al., 2009), the projected stresses of a moving boundary node or interior node can be simply obtained by taking product of the interpolation functions of its sub-domain and the neighboring influencing nodal stresses computed from the EFGM solution within this sub-domain, say,

$$\{\sigma^p\} = [\Psi] \{\sigma\}. \quad (3)$$

In the above, $\{\sigma^p\}$ and $\{\sigma\}$ are the projected stresses and the neighboring influencing nodal stresses by the EFGM solution, respectively. $[\Psi]$ denotes the interpolation functions within the sub-domain for the projected stresses $\{\sigma^p\}$. It is noteworthy that the differences between these projected stresses $\{\sigma^p\}$ and their original stresses $\{\sigma^h\}$ solved from the EFGM can be denoted as a measure of the pointwise errors at this moving boundary node or interior node as follows:

$$\{\sigma^e\} = \{\sigma^p\} - \{\sigma^h\}. \quad (4)$$

The pointwise errors $\{\sigma^e\}$ are generally difficult to indicate and another measure, the so-called L_2 norm, is thus utilized. For stresses, the pointwise error in L_2 norm at this moving boundary node or interior node can be expressed as

$$\|M\| = \left[\{\sigma^e\}^T \{\sigma^e\} \right]^{1/2}. \quad (5)$$

The smoother projected stresses in L_2 norm can be treated as the measure reference and indicated as

$$\|R\| = \left[\{\sigma^p\}^T \{\sigma^p\} \right]^{1/2}. \quad (6)$$

The relative error at this moving boundary node or interior node is thus defined as

$$r = \frac{\|M\|}{\|R\|}. \quad (7)$$

When the relative error r for a moving boundary node or interior node surpasses its tolerance, the interior adaptivity needs to be executed to improve the solution accuracy.

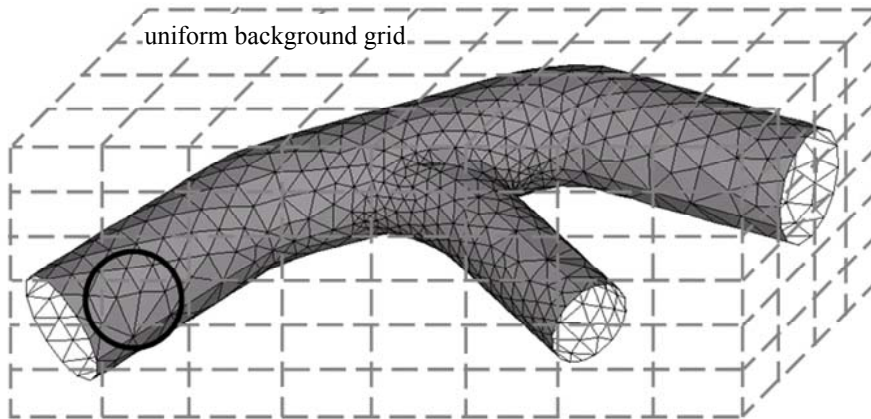
To estimate the error estimation, the nodal displacements/strains/stresses of the moving boundary node and inserted node for adaptivity need to be determined in advance. Hence, a rigorous data mapping procedure based on the MLS approximation is required and adopted in this work. By this data mapping procedure, the undetermined nodal variables for a moving boundary node and new inserted node can be interpolated by its neighboring influencing moving boundary/interior nodes within its sub-domain.

3.2 Surface Adaptive Strategy

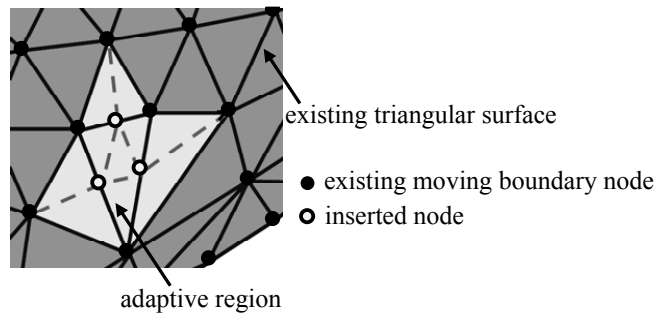
The surface of the analysis domain also needs to be defined in advance for the structural analysis. Nevertheless, since only nodal data are provided by the meshless methods, the geometric information of the analysis domain is inadequate especially for three-dimensional problems with irregular shape. As shown in Fig.4 (a), for example, Lee and Chen (2010) proposed a triangular surface scheme for the meshless methods to represent the surface of three-dimensional irregular geometry. It is worth noting that these triangular surfaces can not only define the geometry, but also serve as an efficient check mechanism. Although the three-dimensional irregular-shaped analysis domain can be successfully described by this scheme, the triangular surfaces on the surface of the analysis domain may be severely distorted when the analysis domain is deformed extremely.

A novel surface adaptivity based on this triangular surface scheme is thus proposed in this work. As illustrated in Fig.4 (b), if the lengths of any two edges of a deformed triangular surface are beyond their respective initial length by a predetermined percentage, say, 50% for all the analyzed problems in the study, 3 new nodes will be inserted at the midpoint of each edge of this triangular surface. This triangular surface to be adapted will be divided into 4 smaller triangular surfaces. To maintain all the existing moving boundary nodes and inserted nodes, the existing triangular surfaces adjacent to the adapted triangular surfaces also need to be divided into 2 smaller ones, as illustrated in Fig.4 (b). Thus, the surface of the analysis domain through this surface adaptive strategy becomes more accurate to represent its deformation and the three-dimensional irregular-shaped analysis domain can be precisely displayed. In addition, the nodal variables of these newly inserted nodes, such as nodal displacements, strains and stresses, can also be obtained through the above-mentioned MLS approximation (Chen et al., 2009) without additional effort.

Besides providing the geometry information of the analysis domain, this triangu-



(a) triangular surface description



(b) triangular surface adaptivity

Figure 4: The surface adaptive scheme with triangular surfaces

lar surface scheme can also be treated as an assistant instrument for determining whether the fictitious nodes or quadrature points are inside the analysis domain or not (Lee and Chen, 2010). Hence, the proposed surface adaptive strategy can reinforce the versatility of the triangular surface scheme (Lee and Chen, 2010) in supplying the precious geometry information for the meshless methods. Consequently, the complex contact behaviors occurred in various engineering problems can be studied rigorously by the proposed surface adaptive strategy.

4 Results and Discussions

To evaluate the efficiency and capability of the novel adaptive strategy with the uniform background grid, two different sorts of three-dimensional deformed problems are sequentially examined. Example 1 is the upsetting of a cylinder between two rigid punches, and example 2 is the simulation for the embossing process of microimprint lithography.

4.1 Upsetting by Two Punches

Consider a cylinder compressed by two rigid punches, of which its radius and length at undeformed state are 10mm and 30mm respectively. The material of the cylinder analyzed is T300 series stainless steel and its mechanical properties are known as: Young's modulus $E=200\text{GPa}$, Poisson's ratio $\nu=0.3$ and ultimate strength 2.14GPa . The bilinear isotropic hardening with yield strength $\sigma_y=0.7\text{GPa}$ and elasto-plastic tangent modulus 0.3GPa are found. Two distinct contact conditions between the cylinder and two rigid punches with different sizes are analyzed. Due to symmetry, only one-eighth of the cylinder is solved for simplicity. The three-dimensional adaptive EFGM analysis model with the uniform background grid as established by Chen et al. (2009) is utilized. Appropriate boundary conditions and a displacement control with 4% reduction in each load increment are applied. After convergence test, two converged ANSYS[®] finite element models, 324 twenty-node isoparametric elements with 1,470 nodes and another delicate model using 594 elements with 2,840 nodes, are presented for comparison. The total reaction force P at the interface between the cylinder and rigid punches is then calculated.

For the case when the interface between the cylinder and rigid punches is sticking, as shown in Fig.5, the cross-section of the rigid punches employed is much larger than that of the cylinder. Therefore, the nodes located at the interface between the cylinder and rigid punches are all fixed in radial direction due to the sticking condition. The relationship between the computed total reaction force P and total reduction δ is then drawn. As observed from Fig.5, the analysis model without adaptivity, as built by Chen et al., 2009, can work only till the total reduction 72% of the cylinder. However, the analysis with the present adaptive strategy can not only improve the analysis well till the total reduction 80% of the cylinder, but also is in better agreement with the converged ANSYS[®] models. In addition, as compared with the ANSYS[®] models, there are much fewer nodes used in the proposed adaptive EFGM model. As the total reduction δ reaches 80% of the cylinder, the number of the moving boundary nodes, interior nodes and inserted nodes become 158, 0 and 189, respectively. This will limit the calculation. Yet, to continue the

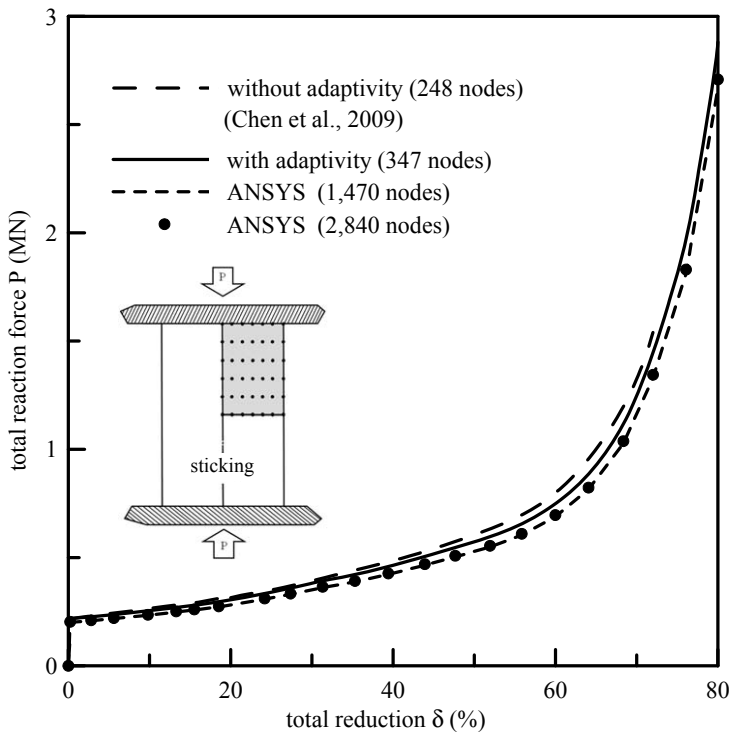


Figure 5: The total reaction force versus the total reduction (sticking)

calculation further, the proposed adaptive model can be executed without difficulty by refining the nodal spacing of the uniform background grid chosen. The maximum von Mises stress computed is 1.61GPa, which is under the ultimate strength 2.14GPa.

For another case when the frictional contact at the interface between the cylinder and rigid punches is concerned, as displayed in Fig.6, the cross-section of the rigid punches is the same as that of the undeformed cylinder. The friction coefficient μ is taken as 0.3. The relationship between the calculated total reaction force P and the total reduction δ is also drawn in Fig. 6. The proposed adaptive strategy is successfully performed till the total reduction 80% of the cylinder, as compared with the total reduction 76% of the cylinder by Chen et al. (2009). Again, the results by the proposed adaptive strategy are more compatible with those by the more elaborate ANSYS[®] model and the inserted nodes introduced by the proposed adaptive strategy can effectively improve the shortcomings by the whole uniform background grid. As would be expected, the lower maximum von Mises stress

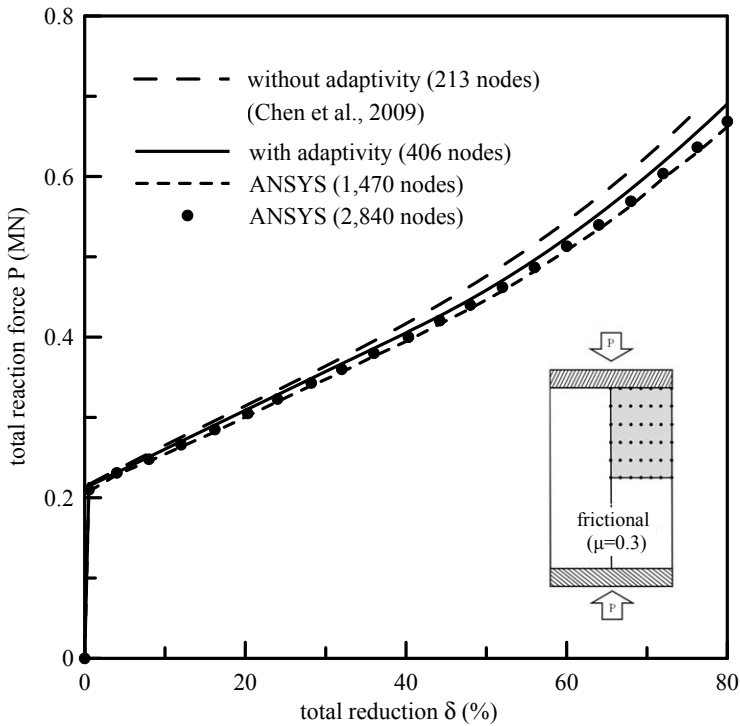
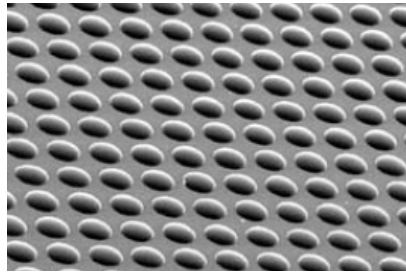


Figure 6: The total reaction force versus the total reduction ($\mu=0.3$)

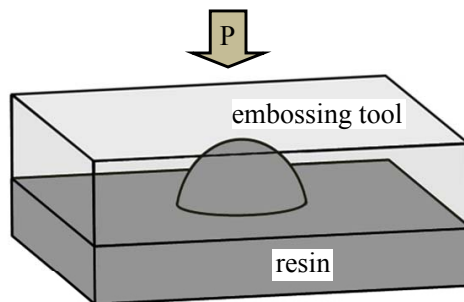
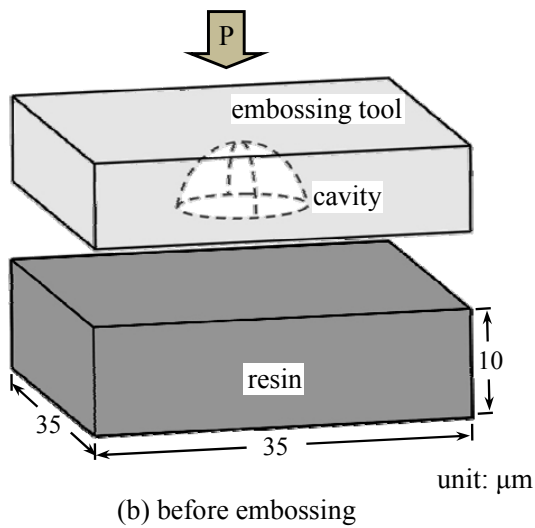
1.43GPa is computed as compared with that for the sticking case. When the total reduction of the cylinder is over 80%, the nodal spacing of the uniform background grid should be refined for further analysis such that more interior nodes can be provided.

4.2 Embossing Process of Microimprint Lithography

Microimprint lithography is an important technique which ensures the high-throughput patterning of microstructures. Since the patterning is periodically symmetric, as shown in Fig.7 (a), only a unit of the patterning is chosen to solve. Consider a three-dimensional resin, of which its length, width and height at undeformed state are $35\mu\text{m}$, $35\mu\text{m}$ and $10\mu\text{m}$, respectively, as depicted in Fig.7 (b). By the embossing process, the resin is compressed by an embossing tool, containing a half spherical cavity with a radius of $6\mu\text{m}$, until the resin is deformed extremely and the half spherical cavity is filled with the resin, as illustrated in Fig.7 (c). The mechanical properties of this resin are: Young's modulus $E=3\text{MPa}$ and Poisson's ratio $\nu=0.49$.



(a) periodically symmetric patterning (Chang et al., 2006)



(c) after embossing

Figure 7: The microimprint lithography: embossing tool, cavity and resin

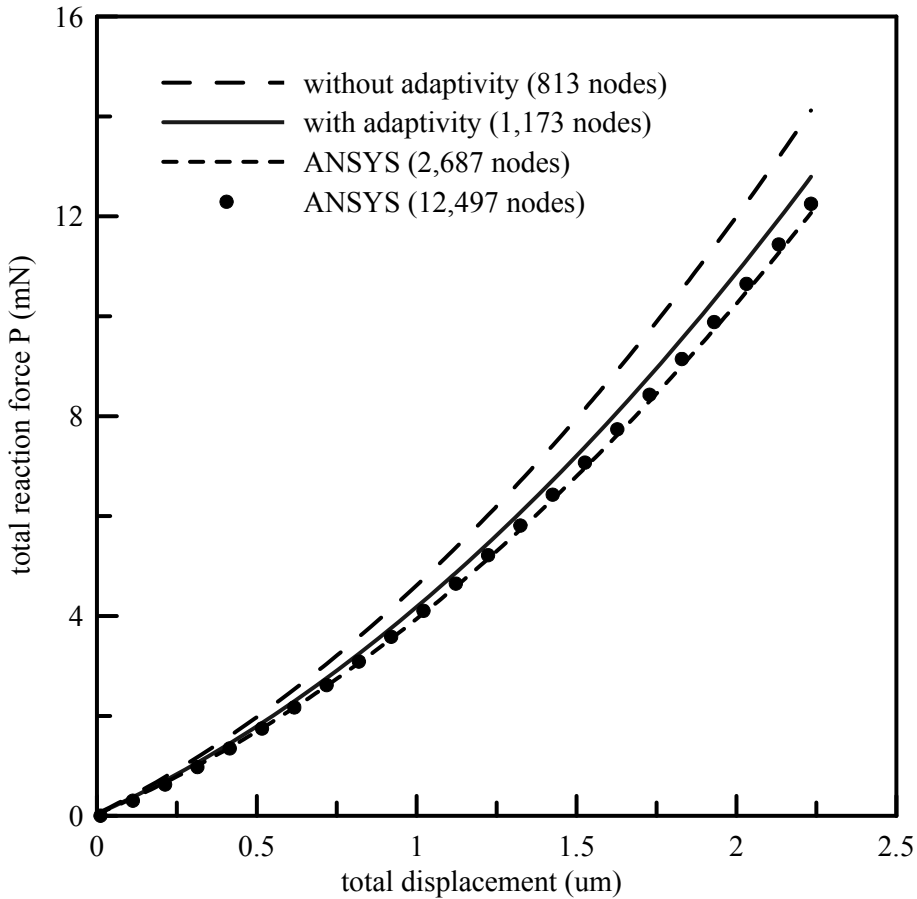


Figure 8: The total reaction force vs. the total displacement

Due to the periodic-symmetry of geometry and boundary conditions, it is adequate to analyze only a quarter of the resin. There are 464 moving boundary nodes and 400 initial interior nodes employed at its initial state. Suitable fixed boundary conditions in the directions perpendicular to the symmetric surfaces of the resin are imposed. To demonstrate the validity of this proposed adaptive strategy, the results by the EFGM analysis without adaptivity are also presented. Besides, two converged ANSYS[®] finite element models, using 13,104 four-node tetrahedral elements with 2,687 nodes and 66,635 elements with 12,497 nodes, are displayed. The relationship between the total reaction force and the total displacement of the embossing tool analyzed by various models is drawn. As seen in Fig.8, the results by the proposed adaptive strategy are in good agreement with those by the deli-

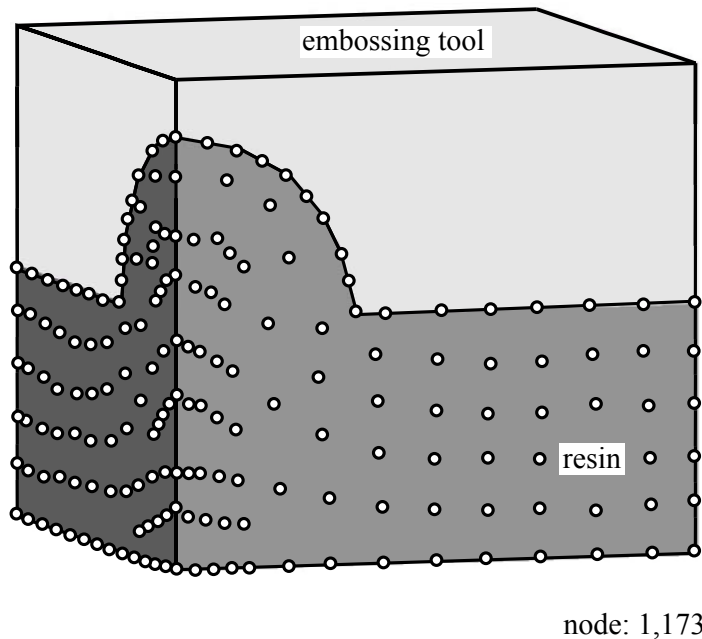


Figure 9: The deformed shape of resin after embossing

cate ANSYS[®] finite element model and are about 10% improvement in calculation as compared with those without adaptivity. The deformed shape of the resin and the nodal distribution after embossing examined by the proposed adaptive EFGM model are also demonstrated in Fig.9. At the final state, there are 1,173 nodes, including 464 moving boundary nodes, 349 interior nodes and 360 inserted nodes.

5 Concluding Remarks

Based on the conventional EFGM analysis, the novel interior and surface adaptive strategies with the uniform background grid have been successfully developed. By the proposed interior adaptive scheme determined by the error estimation, additional adaptive nodes are inserted in the interior regions where the solution needs to be improved. By the proposed surface adaptive strategy, however, the surface adaptive scheme is devised by dividing the original triangular surfaces into smaller triangular surfaces which can describe the irregular three-dimensional geometry precisely. To demonstrate the versatility of this work, the problems of upsetting and embossing are analyzed. It is worthwhile to mention that the proposed adap-

tive strategies with the uniform background grid can also be easily extended to other meshless methods.

Acknowledgement: The authors would like to thank the National Science Council of the Republic of China for financially supporting this research under Contract NSC 98-2221-E-007-017-MY3.

Reference

Atluri, S. N., Zhu, T. (1998): A new meshless local Petrov-Galerkin (MLPG) approach in computational mechanics, *Computational Mechanics*, Vol. 22, pp. 117-127.

Atluri, S. N. (2004): *The Meshless Method (MLPG) for Domain & BIE Discretizations*, 680 pages, Tech Science Press.

Belytschko, T., Lu, Y. Y., Gu, L. (1994): Element-Free Galerkin Method, *International Journal for Numerical Methods in Engineering*, Vol. 37, pp. 229-256.

Chang, C. Y., Yang, S. Y., Huang, L. S., Chang, J. H. (2006): Fabrication of plastic microlens array using gas-assisted micro-hot-embossing with a silicon mold, *Infrared Physics & Technology*, Vol. 48, pp. 163-173.

Chen, W. H., Guo, X. M. (2001): Element Free Galerkin Method for Three-Dimensional Structural Analysis, *Computer Modeling in Engineering & Sciences*, Vol. 2, no. 4, pp. 497-508.

Chen, W. H., Chen, C. H. (2005): On Three-Dimensional Fracture Mechanics Analysis by an Enriched Meshless Method, *Computer Modeling in Engineering & Sciences*, Vol. 8, no. 3, pp. 177-190.

Chen, W. H., Chi, C. T., Lee, M. H. (2009): A Novel Element-Free Galerkin Method with Uniform Background Grid for Extremely Deformed Problems, *Computer Modeling in Engineering & Science*, Vol. 40, no. 2, pp. 175-199.

Chung, H. J., Belytschko, T. (1998): An error estimate in the EFG method, *Computational Mechanics*, Vol. 21, pp. 91-100.

Chung, H. J. (2000): Adaptive nodal generation with the element-free Galerkin method, *Structural Engineering and Mechanics*, Vol. 10, pp. 635-650.

Jun, S., Im, S. (2000): Multiple-scale meshfree adaptivity for the simulation of adiabatic shear band formation, *Computational Mechanics* Vol. 25, pp.257-266.

Lee, M. H., Chen, W. H. (2009): A three-dimensional meshless scheme with background grid for electrostatic-structural analysis, *Computers, Materials and Continua*, Vol.11, No.1, pp.59-77.

Lee, M. H., Chen, W. H. (2010): Geometry-related Treatments for Three-dimensional

Meshless Method, *Computer Modeling in Engineering and Sciences*, Vol.61, No.3, pp.249-271.

Li, S., Atluri, S. N. (2008): The MLPG Mixed Collocation Method for Material Orientation and Topology Optimization of Anisotropic Solids and Structures, *Computer Modeling in Engineering & Sciences*, Vol. 30, no.1, pp. 37-56.

Li, Q., Lee, K.-M. (2006): An adaptive meshless method for magnetic field computation, *IEEE Transactions on Magnetics*, Vol. 42, no. 8, pp. 1996-2003.

Liu, G. R., Tu, Z. H. (2002): An adaptive procedure based on background cells for meshless methods, *Computer methods in applied mechanics and engineering*, Vol. 191, pp. 1923-1943.

Liu, G. R., Kee, B. B. T., Chun, Lu. (2006): A stabilized least-squares radial point collocation method(LS-RPCM) for adaptive analysis, *Computer methods in applied mechanics and engineering*, Vol. 195, pp. 4843-4861.

Lu, H., Chen, J. S. (2002): Adaptive Galerkin particle methods, *Lecture Notes in Computer Science*, Vol. 26, pp. 251-267.

Nagashima, T. (2000): Development of a CAE system based on the node-by-node meshless method, *Computer methods in applied mechanics and engineering*, Vol. 187, pp. 1-34.

Rabczuk, T., Belytschko, T. (2005): Adaptivity for structured meshfree particle methods in 2D and 3D, *International journal for numerical methods in engineering*, Vol. 63, pp. 1559-1582.

Rabczuk, T., Belytschko, T. (2007): A three-dimensional large deformation mesh-free method for arbitrary evolving cracks, *Computer methods in applied mechanics and engineering*, Vol. 196, pp. 2777-2799.

Rossi, R., and Alves, M. K. (2005): An h -adaptive modified element-free Galerkin method, *European Journal of Mechanics A/solids*, Vol. 24, pp. 782-799.

You, Y., Chen, J. S., Ku, H. (2003): Filters, reproducing kernel, and adaptive meshless method, *Computational Mechanics*, Vol. 31, pp. 316-326.

Yvonnet, J., Cofignal, G., Ryckelynck, D., Lorong, Ph., Chinesta, F. (2006): A simple error indicator for meshfree methods based on natural neighbors, *Computers and Structures*, Vol. 84, pp. 1301-1312.

Zhang, Z. Q., Zhou, J. X., Wang, X. M., Zhang, Y. F., Zhang, L. (2005): h -Adaptivity Analysis Based on Multiple Scale Reproducing Kernel Particle Method, *Applied Mathematics and Mechanics*, Vol. 26, No. 8, pp.1064-1071.